Hong Kong J Radiol. 2015;18:27-36 | DOI: 10.12809/hkjr1414262

ORIGINAL ARTICLE **CME**

Computed Tomography and Magnetic Resonance Imaging of Adenolymphoma (Warthin's Tumour) of the Parotid Gland

AK Yadav[1], CC Xia[1], YF Peng[1,2], HD Shao[1], XZ Gang[1]

[1]Department of Radiology, Shanghai 10th People's Hospital of Tongji University, Shanghai, China;
[2]Department of Radiology, Shanghai Putuo Hospital of Traditional Chinese Medicine, Shanghai, China

ABSTRACT

Objective: *To characterise the computed tomography / magnetic resonance imaging (CT/MRI) features to diagnose adenolymphoma (Warthin's tumour).*

Methods: *Between February 2008 and December 2012, CT/MRI scans of consecutive patients referred for suspected parotid tumours were performed before surgery or fine-needle aspiration cytology. All patients underwent surgery and samples were sent for pathological confirmation of the diagnosis. Their CT/MRI scans with pathologically proven Warthin's tumours were reviewed.*

Results: *All of the 17 patients in the study were men, and aged between 43 and 86 years (mean, 65 years). All the patients initially presented with gradually increasing painless masses, with duration of symptoms ranging from 1 month to 120 months (mean, 61 months). Two patients were found to have bilateral Warthin's tumour, nine had a left-sided Warthin's tumour, and six had a right-sided Warthin's tumour.*

Conclusion: *The CT/MRI findings were helpful in distinguishing these benign lesions from other parotid gland tumours when biopsy results are non-diagnostic. Further studies are needed to assess the positive predictive value of the imaging features.*

Key Words: *Adenolymphoma; Magnetic resonance imaging; Tomography, X-ray computed*

中文摘要

腮腺腺淋巴瘤（沃辛瘤）的電腦斷層掃描和磁共振成像（CT/MRI）

AK Yadav、夏琛琛、彭屹峰、邵鴻達、鋼熊炸

目的：介定腮腺腺淋巴瘤（沃辛瘤）的CT/MRI診斷特徵。

方法：2008年2月至2012年12月期間，所有腮腺腫瘤疑似病例均於術前或在細針穿刺抽吸活檢前作CT/MRI檢查。所有病人均接受手術，其活檢樣本經病理學檢查，並回顧研究確診為腮腺沃辛瘤病例的CT/MRI。

結果：被納入研究的17例全為男性，年齡介乎43歲至86歲，平均65歲。所有患者初發症狀為體積逐漸增大的無痛性腫塊，持續1至120個月（平均61個月）。其中2例雙側腮腺沃辛瘤，另9例左側腮腺沃辛瘤，6例右側腮腺沃辛瘤。

Correspondence: *Prof YF Peng, Department of Radiology, Shanghai 10th People Hospital of Tongji University, Yanchang Road-301, Shanghai-200072, China; Shanghai Putuo Hospital of Traditional Chinese Medicine, Shanghai-200062, China.*
Email: peng2188@sina.com; mr_arunosome@yahoo.com

Submitted: 26 Aug 2014; Accepted: 7 Nov 2014.

結論：如未能根據活檢結果作出診斷時，CT/MRI能將此類良性病變與其他腮腺腫瘤區分開來。但須進一步研究這些影像學特徵對沃辛瘤的陽性預測值。

INTRODUCTION

Adenolymphoma (Warthin's tumour) is a benign tumour of the salivary gland, which is predominantly found in the parotid gland. Warthin's tumour was initially described in 1929 and named after the pathologist Aldred Scott Warthin.[1] It is also known as papillary cystadenoma lymphomatosum, adenolymphoma, cystadenolymphoma, and papillary cystadenoma. It is a fairly common tumour, accounting for 14% to 30% of parotid tumours, and is well-known among otolaryngologists. Unlike benign mixed tumours, Warthin's tumour recurs in less than 2% of patients and only 1% of patients develop a malignant tumour. More men develop Warthin's tumour than women, at a ratio of 5:1.[2] Warthin's tumour is most commonly diagnosed incidentally on computed tomography (CT) scan. The tumour usually occurs in older patients, most often in the sixth and seventh decades of life.[3]

There are several hypotheses concerning Warthin's tumour, but the widely accepted explanation describes it as a condition that develops from the hyperplasia of the salivary duct cells isolated in the lymph node of the parotid gland during embryogenesis. Other theories suggest that Warthin's tumour is caused by the infiltration of lymphocytes inside an existing adenoma or interaction of hyperplasia of glandular epithelium and excessive lymphoid tissue inside the stroma.[4,5]

The most common presentation is that of an asymptomatic mass (81%) noted incidentally while washing or shaving the face. Pain and facial nerve palsy occur less frequently. While painful masses may be produced by obstructive or inflammatory disease, a classic painless mass in the parotid gland is usually due to a neoplasm, cyst, or lymph node.[6] Local excision or superficial parotidectomy is established as the surgical procedures of choice. Most Warthin's tumours of the parotid gland are slow-growing, with smooth well-defined margins.

Preoperative imaging has assumed a major role in surgical planning for assessing the location of a tumour. It is useful to understand the typical CT/magnetic resonance imaging (MRI) features of Warthin's tumour. The purpose of this study was to assess patients suspected to have Warthin's tumour to detect specific imaging findings to provide more accurate diagnosis. Imaging of the parotid glands has two purposes: first, to establish the precise extent and site of any parotid lesions; and, second, to provide some indications of its pathological nature. It is important to determine whether a parotid gland tumour is benign or malignant. CT could identify patients with pleomorphic adenomas, Warthin's tumours, or malignant tumours, and evaluate the extent of any parotid gland tumours. Moreover, detailed information on signal intensity and washout ratio in a parotid gland tumour by contrast-enhanced MRI has been reported for pleomorphic adenomas, Warthin's tumours, and malignant tumours. Hence CT/MRI with histopathology gives promising results for diagnosis of Warthin's tumour.

METHODS

Patients

Between February 2008 and December 2012, CT and MRI scans of consecutive patients referred for suspected parotid tumours were performed before surgery or fine-needle aspiration cytology. All patients underwent surgery and samples were sent for pathological confirmation of the diagnosis. The CT/MRI scans of all patients with pathologically proven Warthin's tumours were reviewed. This study was approved by the local ethics committee.

Imaging Techniques and Image Analysis

A 4-slice CT unit (GE Healthcare, Wauwatosa [WI], USA) and 3.0 T MRI unit (Siemens, Erlangen, Germany) with a neck coil were used. The CT images were reconstructed at 3- to 5-mm thickness in both the axial and coronal planes. The section thickness and pitch factor were in the ranges of 3 to 5 mm and 1 or <1, respectively. Images were acquired at 120 kV and 200 mA, with a total scanning time of 35 seconds. An intravenous bolus dose of 70 ml of non-ionic contrast (iohexol, 350 mg I/ml) was administered to patients at an injection rate of 2.5 ml/s.

The MRI examination included multiplanar images. The minimum sequences are shown in Table 1. Two board-certified radiologists (sub-specialised in head and neck radiology) evaluated the CT/MRI scans according to

Table 1. Specifications of multiplanar images.

	Axial T1-weighted	Axial T2-weighted	Coronal T2-weighted	Axial gadolinium-enhanced T1-weighted
Repetition time (ms)	650	4540	4540	802
Echo time (ms)	10	90	96	10
Section thickness (mm)	4	4	4	4
Field of view (mm)	230	230	220	230
Resolution (matrix)	320 x 224	320 x 237	320 x 256	320 x 224
Voxel size (mm)	1.0 x 0.7 x 4.0	0.9 x 0.7 x 4.0	0.9 x 0.7 x 4.0	1.0 x 0.7 x 4.0

the tumour location, size, margins, contour, attenuation and signal intensity, and enhancement pattern. The lesion margins (well-defined or ill-defined), size (long- and short-axis diameters measured on axial images), location (superficial or deep), and contour (smooth or lobulated) were recorded. A virtual line was drawn from the lateral border of the posterior belly of the digastric muscles and retromandibular vein to the lateral edge of the mandible to locate the superficial and deep lobes.[7] The CT attenuation was compared with that of the adjoining skeletal muscles and tissues.

Signal on T1-weighted images was judged as low (iso-to-low signal or hypointensity) when the signal of the parotid gland was equal or lower than the signal of muscle, high (high signal or hyperintense) when the signal was brighter than muscle, and strong (highly hyperintense) when the signal was closer to that of water (cerebrospinal fluid) than that of the parotid gland. T2-weighted and turbo-inversion recovery magnitude characteristics were reported as low (hypointense) when the signal of the tumour was lower than that of parotid tissue, high (hyperintense) when the signal was equal to or brighter than that of normal parotid tissue, and strong (highly hyperintense) when the signal was closer to that of water (cerebrospinal fluid) than that of parotid tissue. The tumour texture was recorded as heterogeneous or homogeneous in attenuation and high-signal intensity. On MRI, the tumour texture was based on the appearance of the lesions on T2-weighted imaging. Appearance was classified as lobulated and cystic / necrotic with areas without enhancement. The approximate tumour volume was calculated by using the product of tumour length, width, and depth. Furthermore, the tumour appearance was classified into homogeneous and heterogeneous, and obvious and non-obvious on both pre- and post-contrast sequences.

RESULTS

All 17 patients were men, and aged between 43 and 86 years (mean, 65 years). All the patients initially presented with gradually increasing painless masses, with a duration of symptoms ranging from 1 month to 120 months (mean, 61 months). Two patients were found to have bilateral Warthin's tumour, nine had left-sided Warthin's tumour, and six had right-sided Warthin's tumour. No patients had multiple lesions. The parotid gland was grouped into deep and superficial lobes, which were bounded with the line linking the retromandibular vein and inner sternocleidomastoid as the boundary, and the upper and lower poles were bound with the ear lobe. The clinical profile, imaging findings, and final diagnosis of Warthin's tumour are shown in Table 2.

Location

The tumours were located in the parotid space containing the facial nerve, retromandibular vein, external carotid artery, and intraparotid lymph node. Ten tumours were located at the superficial lobe (5 left-sided, 3 right-sided, and 2 were bilateral [Figure 1]) and seven were in the deep lobe of the parotid gland (4 left-sided and 3 right-sided, with no bilateral deep lobe tumours).

Shape, Size, and Numbers

All of the tumours had sharp well-defined margins, and were with oval-to-round shape. Eleven tumours had smooth margins, one was cystic, three were lobulated, three were both solid and cystic. The mean long-axis diameter was 2.34 cm (range, 1.20-3.40 cm), and the average short-axis diameter was 2.88 cm (range, 1.20-6.00 cm).

Texture and Enhancement

On plain CT, three tumours were hyperdense with heterogeneity, among which one had haemorrhagic necrosis (20 HU) [Figure 2]. On CT with contrast, seven tumours were hyperdense with homogeneity, among which one was found to be hyperdense with heterogeneity. One patient had both CT and MRI

Table 2. Clinical profile, imaging findings, and final diagnosis of patients with parotid tumour.

Patient No.	Age (years) / sex	Modality CT or MRI	Tumour				CT enhancement (HU) AP: 25 seconds DP: 60 seconds V (max FOV) / MRI enhancement	Diagnosis (histopathology)
			Location	Size (cm)	Margin	Contour		
1	43 / M	CT+C	Superficial; left	2.5 x 3.0 x 4.0	Well-defined	Lobulated, uniform hyperdensity	Obvious uniform enhancement V 45,VP V 70, DP V 65	Adenolymphoma
2	66 / M	CT+C	Superficial; left	2.9 x 2.5 x 3.0	Well-defined	Smooth, solid and cystic, heterogeneous hyperdensity	Obvious uniform enhancement (solid part) V 45, VP V 80, DP V 66	Adenolymphoma
3	58 / M	CT+C	Deep; left	2.5 x 2.5 x 3.5	Well-defined	Smooth, cystic with wall nodularity	Nodule has obvious enhancement V 30, VP V 60, DP V 45	Adenolymphoma
4	56 / M	CT+C	Superficial; bilateral	Left: 2.0 x 2.0 x 2.6 Right: 2.0 x 2.1 x 3.0	Well-defined	Smooth, homogeneous high density	Obvious enhancement V 45, VP V 90, DP V 75	Adenolymphoma
5	73 / M	CT+C	Superficial; left	2.2 x 2.5 x 3.5	Well-defined	Lobulated, uniform high density	Obvious enhancement V 38, VP V 75, DP V 68	Adenolymphoma
6	58 / M	CT+C	Superficial; bilateral	Left: 2.0 x 1.5 x 3.5 Right: 1.2 x 0.8 x 1.5	Well-defined	Smooth, uniform high density	Obvious enhancement V 35, VP V 65, DP V 56	Adenolymphoma
7	73 / M	CT+C	Deep; left	1.8 x 2.0 x 2.5	Well-defined	Smooth, homogeneous high density	Obvious enhancement V 40, VP V 75, DP V 65	Adenolymphoma
8	73 / M	CT+C	Superficial; right	1.6 x1.5 x2.5	Well-defined	Smooth, homogeneous iso-to-high density	Obvious enhancement V 35, VP V 75, DP V 55	Adenolymphoma
9	76 / M	MRI+C	Superficial; right	1.6 x 1.5 x 1.8	Well-defined	Smooth, homogeneous iso signal on T1-weighted and high signal on T2-weighted	Obvious and uniform enhancement Fast in and fast out	Adenolymphoma
10	61 / M	MRI+C	Superficial; left	1.6 x 1.5 x 2.6	Well-defined	Smooth, homogeneous low signal on T1-weighted and high signal on T2-weighted	Obvious and uniform enhancement Fast in and fast out	Adenolymphoma
11	62 / M	MRI+C	Deep; right	3.3 x 3.0 x 3.5	Well-defined	Smooth, solid and cystic, low-to-iso signal on T1-weighted and non-homogeneous high signal on T2-weighted	Solid part well-enhanced	Adenolymphoma
12	62 / M	MRI+C	Deep; right	3.4 x 3.0 x 3.5	Well-defined	Smooth, solid and cystic, iso signal on T1-weighted and non-homogeneous high signal on T2-weighted	Solid part obvious enhancement	Adenolymphoma
13	68 / M	MRI+C	Deep; right	1.5 x 1.7 x 2.5	Well-defined	Smooth, slight high signal on T1-weighted and homogeneous high signal on T2-weighted	Obvious homogeneous enhancement	Adenolymphoma
14	54 / M	MRI+C and CT	Superficial; left	3.2 x 2.5 x 3.5	Well-defined	Lobulated, cystic non-homogeneous slight high signal on T1-weighted and non-homogeneous high signal on T2-weighted	Solid part obvious enhancement V 45	Adenolymphoma
15	55 / M	CT	Superficial; right	1.2 x 1.3 x 2.0	Well-defined	Heterogeneous hyperdensity	V 40	Adenolymphoma
16	72 / M	CT	Deep; left	3.5 x 3.0 x 6.0	Well-defined	Necrosis and haemorrhage in lesion, heterogeneous hyperdensity	V 40 Necrosis V 20	Adenolymphoma
17	86 / M	CT	Deep; left	3.0 x 2.6 x 3.0	Well-defined	Heterogeneous hyperdensity with calcification	V 40	Adenolymphoma

Abbreviations: AP = arterial phase; CT/MRI = computed tomography/magnetic resonance imaging; CT+C = computed tomography with contrast; DP = delayed phase; FOV = field of view; MRI+C = magnetic resonance imaging with contrast; V = CT attenuation value; VP = venous phase.

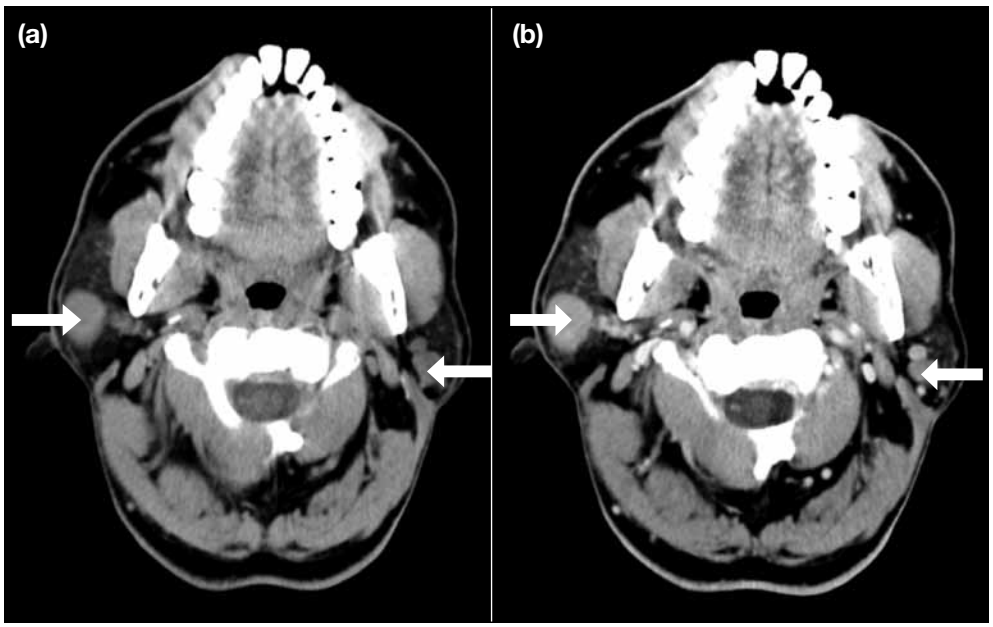

Figure 1. Computed tomography images of a 56-year-old man (patient No. 4) with bilateral neck mass for 10 years: (a) plain axial view shows bilateral homogeneous masses with well-defined margins located superficially (arrows) and (b) view with contrast shows bilateral homogeneous tumours with obvious enhancement (arrows).

Figure 2. A computed tomography image of a 72-year-old man (patient No. 16) with a left-sided neck mass: axial view shows a deep lobe heterogeneous parotid lesion with well-defined margins, with high density (haemorrhage) and low density (necrosis/cyst: 3.5 x 3.0 x 6.0 cm) inside the tumour (arrow).

showing cystic, lobulated tumour with high intensity and hyperdensity (Figure 3). Most of CT scans showed smooth, solid, cystic, lobulated tumours with well-defined margins. One patient demonstrated hyperdensity, heterogeneous with calcification on plain CT. Among five MRI patients all showed smooth, homogeneous intensity; the T1-weighted MRI showed iso-to-low signals whereas high signal was shown on T2-weighted images (Figure 4). Gadolinium enhancement was marked, but homogeneous.

All patients in this study underwent surgery, either partial or total parotidectomy depending on the location of the tumours, and a sample was sent for histopathology diagnosis. No clinical evidence of local tumour recurrence has been detected.

DISCUSSION

Parotid is a Greek word that means 'near the ear'. The parotid glands are the largest of the salivary glands. They are paired glands that contain mucus and serous cells, and a ductal network. A parotid mass is a common clinical presentation in head and neck imaging. In adults, benign tumours such as pleomorphic adenoma or Warthin's tumour are the most common diagnoses.[8] In the past, Warthin's tumour was seen primarily in white men, but it is becoming more prevalent both in African Americans and in women. Although Warthin's tumour can occur elsewhere, it is most commonly found in the parotid gland. In one series, all of the Warthin's tumours were located in the parotid gland.[9] Another series found 90% of Warthin's tumours within the parotid gland, 7.6% in the cervical lymph nodes, and 2.3% in the submandibular gland.[10]

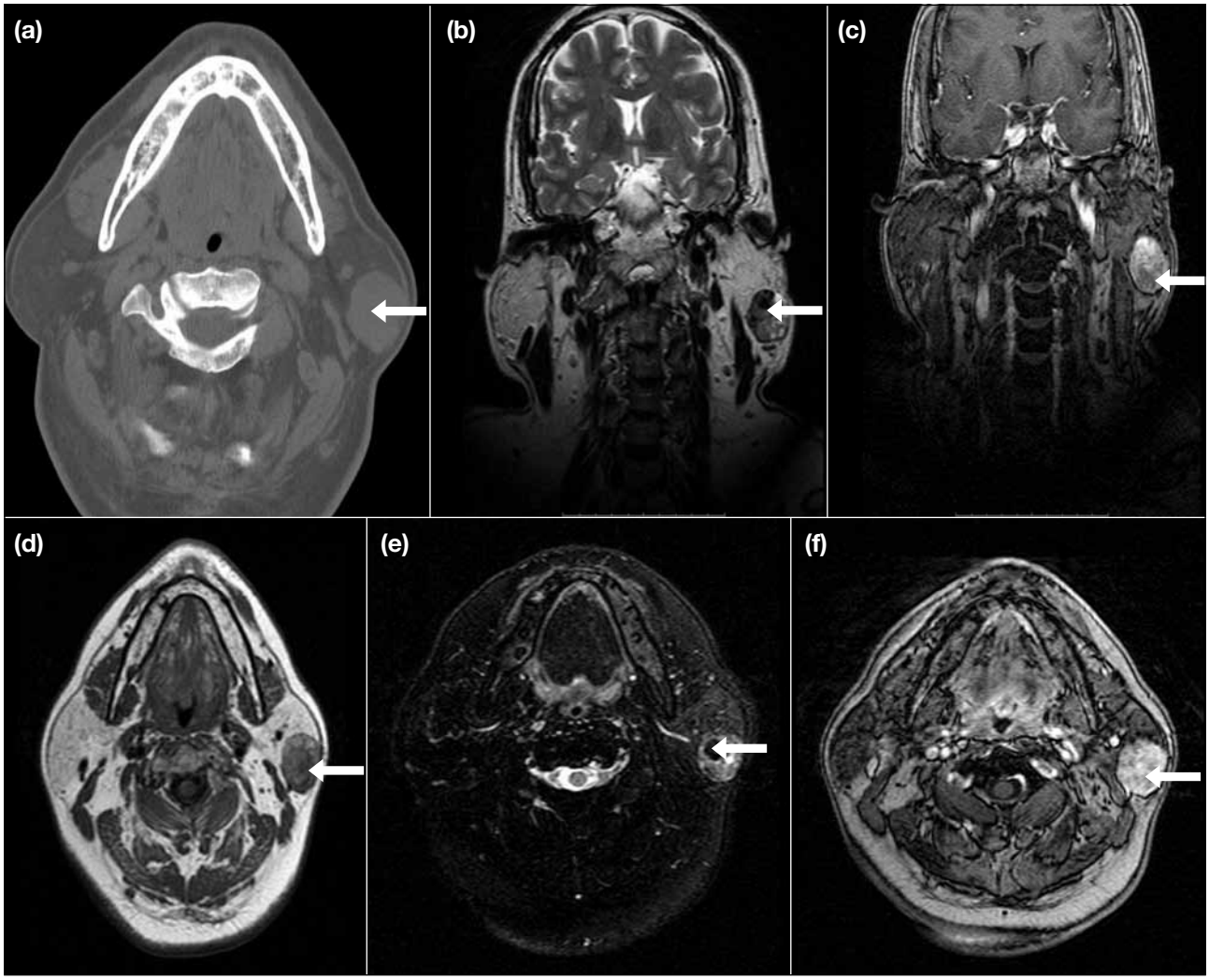

Figure 3. Computed tomography (CT) and magnetic resonance (MR) images of a 54-year-old man (patient No. 14) with a left-sided neck mass: (a) plain axial CT image shows a superficial lobe left-sided mass with well-defined margins (arrow), with isodensity, (b) Coronal T2-weighted MR image shows iso-to-high signal (arrow), (c) Coronal post-contrast T1-weighted MR image shows obvious enhancement of the heterogeneous mass (arrow), (d) axial T1-weighted MR image shows iso-to-high signal with haemorrhagic mass (3.2 x 2.5 x 3.5) [arrow], (e) axial T1-weighted fat-saturated MR image shows high signal mass (arrow) with a small low signal lesion inside suggestive of old haemorrhage (arrow), and (f) axial post-contrast T1-weighted MR image shows obvious enhancement of the superficial lobe heterogeneous mass with clear margins (arrow).

Warthin's tumour is the most frequent monomorphic adenoma of the major salivary glands. Clinically, Warthin's tumour appears as a slow-growing tumour, which is often fluctuant on palpation due to its cystic nature. Warthin's tumour is the second most common benign parotid gland neoplasm in adults and children. This tumour is the most common neoplasm that manifests as multiple lesions, and is bilateral in up to 10% of cases. The most accepted hypothesis about the origin of Warthin's tumour is that it develops from salivary duct inclusions in the lymph nodes after embryonic development of the parotid gland.[11] Benign tumours have only rarely been associated with cigarette smoking, which focuses attention on the nature of the underlying neoplastic process and how it may differ from other benign tumours but, according to Kotwall,[12] smokers have 8 times the risk of developing Warthin's tumour. Although generally believed to be an adenoma, Allegra[13] suggested that Warthin's tumour may be a delayed hypersensitivity reaction.

Warthin's tumour is an adenoma with a variable number of cysts filled with mucoid or brown fluid. The cysts are lined with papillary proliferations of double-layered

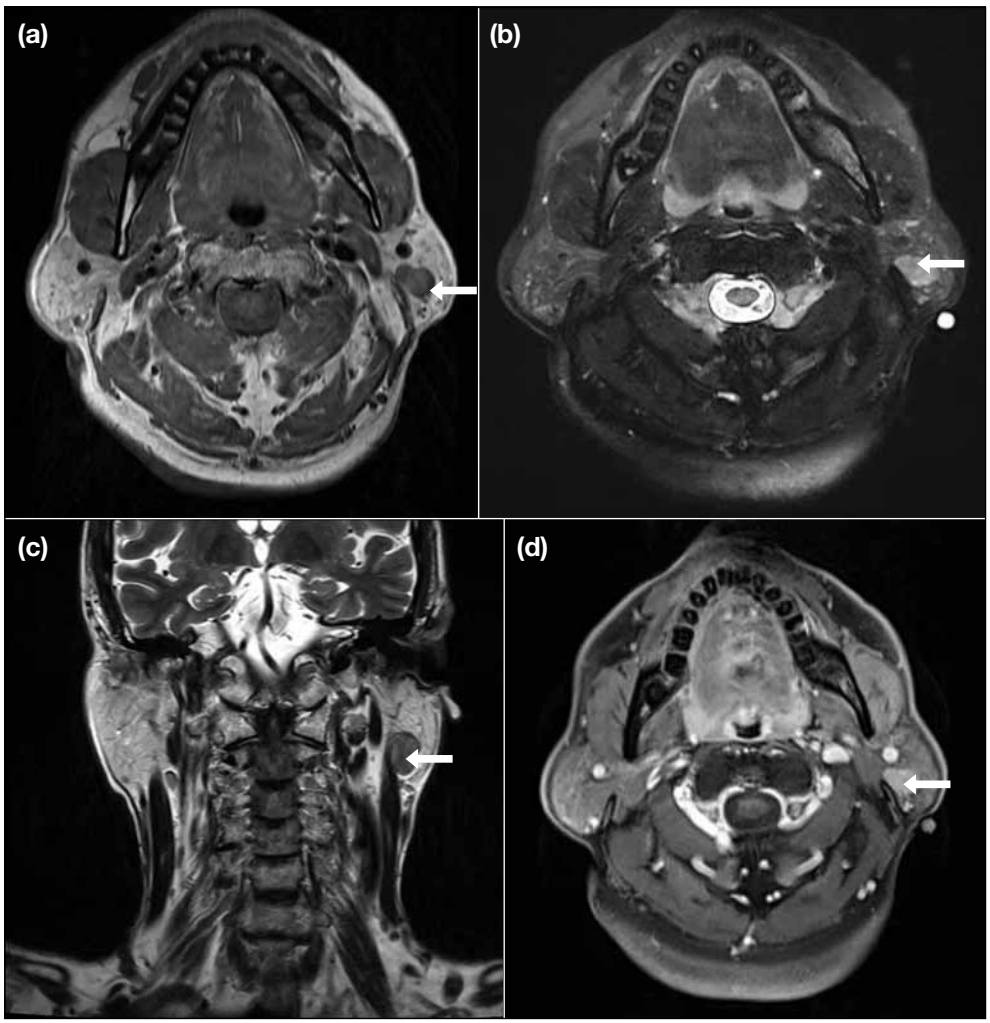

Figure 4. Magnetic resonance images of a 61-year-old man (patient No. 10) with Warthin's tumour with no specific clinical manifestations: (a) axial T1-weighted turbospin-echo image shows a left posterior homogeneous parotid gland mass with iso-low signal with clear margins (arrow), (b) axial T2-weighted turbospin-echo image shows a left parotid gland mass with clear margins and high signal lesion (arrow), (c) coronal T2-weighted turbospin-echo image shows a left parotid gland tumour with slight high signal with clear margins (arrow), and (d) axial post-contrast T1-weighted image shows a left superficial lobe parotid gland tumour with high intensity signal with clear margins (arrow).

oncocytic epithelium and supporting stroma composed of great amounts of follicle-containing lymphoid tissue (Figure 5). The tumour occasionally contains focal haemorrhage and necrosis. Parotidectomy is the most widely accepted surgical treatment for parotid tumour removal.[14] The most serious complications of surgical treatment include facial nerve dysfunction, Frey's syndrome, and local recurrences.

CT and MRI depict the mass, and the findings may be diagnostic in routine cases with typical features. CT is the method of choice for imaging patients suspected to have inflammatory disease (abscess, calculi, major salivary duct dilation, or acute inflammation) or for patients with a contraindication for MRI. For CT imaging, both pre- and post-contrast studies must be performed in order to detect calcification (Figure 6).[15] MRI is the method of choice for imaging patients with palpable masses for whom there is a strong suspicion that the lesion is neoplastic. MRI gives information on the exact localisation and extent of the lesions and addresses neighbouring structures. Ultrasound (US) is a useful technique to assess superficial parotid, submandibular, and sublingual masses. US, however, shows a lack of specificity for cystic lesions and deep lobe evaluation, and the relationship of a tumour to the facial nerve is difficult for surgeons to appreciate on US images.[16,17] Ultrasound has been able to identify a Warthin's tumour based on echo structure, margins, and vascularity.[18,19] CT helps in identifying the structure, margins, number of lesions, pattern of enhancement, washout timeframes, and attenuation coefficients to differentiate between various parotid lesions.[3] On CT and MRI, Warthin's tumour typically appears well-circumscribed with homogeneous, cystic, or solid lesions in the parotid or periparotid region, most

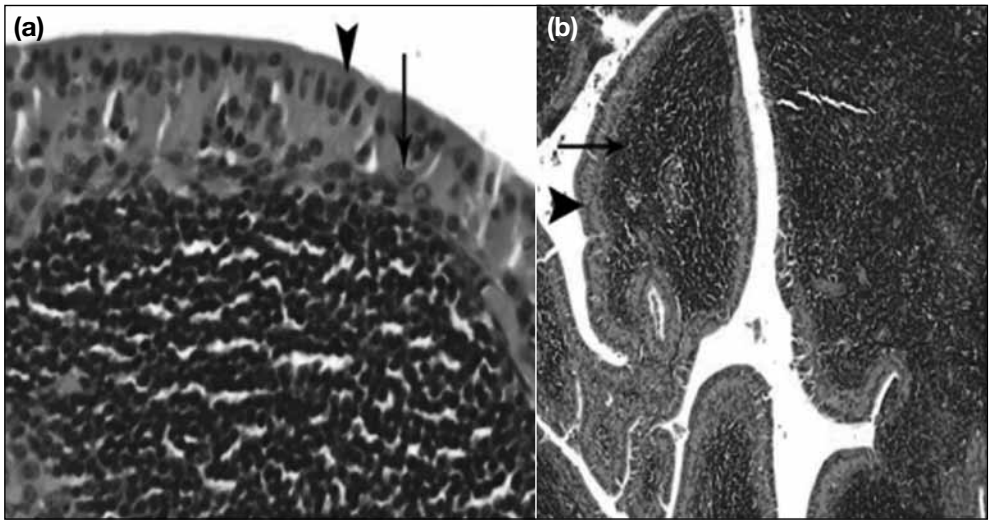

Figure 5. Histopathology of a parotid mass: (a) surface epithelium consists of a double layer, the top layer of tall columnar oncocytic cells (arrowhead) and a basal layer of polygonal cells (arrow) [H&E; original magnification, x 400]. (b) Tumour is multifocal and bilateral with the same frequency. Note the tall columnar cells (arrowhead) enclosing the lymphoid stroma (arrow) [H&E; original magnification, x 100].

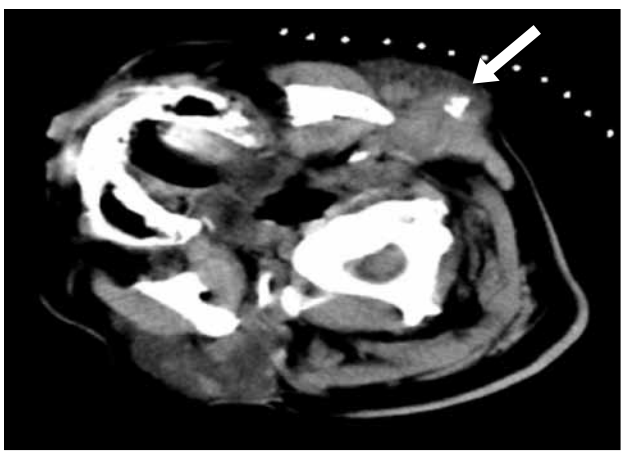

Figure 6. An axial computed tomography image of an 86-year-old man (patient No. 17) with a left-sided deep lobe parotid mass shows well-defined margins with a calcified lesion (arrow).

commonly involving the inferior pole of the gland. The appearance of multiple or bilateral parotid or periparotid masses is suggestive of a Warthin's tumour.

Although MRI is more commonly used to evaluate parotid masses, CT imaging has also shown promise in elucidating parotid masses. MRI is an established way of showing the morphology and extent of head and neck tumours and their adjacent structures. However, it is commonly thought that MRI cannot make a reliable distinction between benign and malignant neoplasms. The important differential diagnoses for well-defined enhancing parotid tumours seen on CT include Warthin's tumour and basal cell adenoma. Warthin's tumour shows enhancement in the early post-contrast scan phase, but decreased enhancement in the delayed phase.[20] On the basis of Bryan et al's study,[21] CT done with a high-resolution CT scanner is the initial radiographic procedure of choice for evaluating salivary gland masses, particularly if neoplasm is the primary consideration. For Warthin's tumour, 89% of foci are enhanced markedly in the early stage and decrease in density in the late stage (120 seconds), therefore, delayed enhancement is not seen. A malignant parotid tumour shows irregular appearance, easy haemorrhage, necrosis and crystallisation, and infiltrative growth. A malignant parotid tumour is apt to induce injury of the facial nerve, facial paralysis, and regional nodal metastasis.[22] The parotid Warthin's tumour in all of the patients in this study had sharp well-defined margins.

Warthin's tumours are usually diagnosed in elderly men, with 10% to 15% having synchronous bilateral disease.[20] There is an overlap of radiologic features between Warthin's tumour and other benign tumours such as oncocytoma and basal cell adenoma and, to a lesser degree, pleomorphic adenoma. Benign parotid Warthin's tumour usually occurs in the sixth decade of life and mainly in men, who present with CT or MRI findings of well-defined margins, solid, cystic, lobulated, well-circumscribed, homogeneous lesions (Figure 7). These findings are atypical for pleomorphic adenoma. A study by Choi et al[23] found

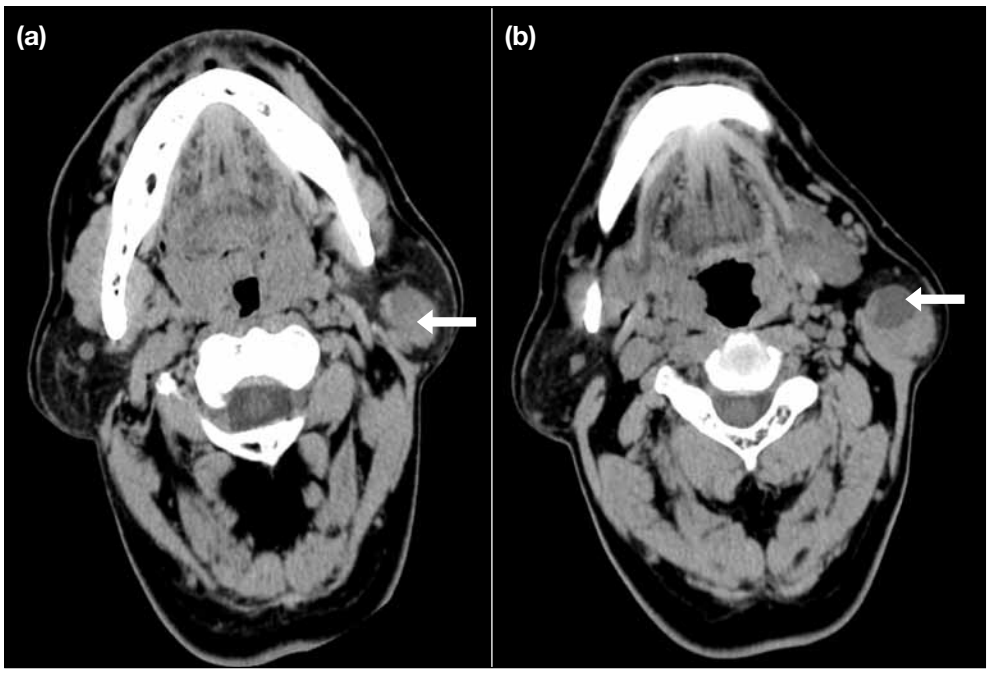

Figure 7. Computed tomography images of a 58-year-old man (patient No. 3) with a left-sided deep lobe parotid mass. (a) An axial image shows the mass with clear margins (arrow) and (b) with iso-density indicating a cystic lesion (arrow) [15 HU: 2.5 x 2.5 x 3.5 cm].

that Warthin's tumour (8 out of 9) showed strong early phase enhancement with a decrease in attenuation on delayed imaging (120 seconds) as opposed to the signs for pleomorphic adenoma (30 out of 35) which showed increased delayed enhancement.[3] A 30% washout ratio threshold can be useful for predicting whether parotid gland tumours are benign or malignant. Warthin's tumours typically demonstrate ≥30% washout, whereas malignant tumours demonstrate low washout of <30% and complicated cysts show early enhancement and low washout ratio (≤30%). Ikeda at al[24] had similar findings with 44.0% (standard deviation [SD], 20.4%) average washout ratio of Warthin's tumour compared with malignant tumours, which had a washout ratio of 11.9% (SD, 11.6%). According to Sakamoto et al,[25] a heavy T2-weighted sequence can help to distinguish a pleomorphic adenoma (which usually appears more heterogeneous) from a Warthin's tumour (which usually appears more homogeneous). The protocol for MRI of parotid gland lesions consists of four imaging sequences in addition to sagittal localising images. The most important images are axial T2-weighted images and axial and coronal contrast-enhanced fat-suppressed images. To obtain optimal delineation of a tumour, we use 3-mm sections through the gland, with a gap of 0.5 mm or 1.0 mm between sections.[26] This allows evaluation of the tumour margins as well as the relationship of the tumour to the ramus of the mandible, muscles of mastication, and retromandibular vein.

CONCLUSIONS

For middle-aged or older men with a smoking history, if they have painless foci in the superior and deep parts of the parotid gland showing a clear boundary, significant enhancement, and uniform or non-uniform density / signal with moderate or significant enhancement, especially for unilateral or bilateral foci, parotid Warthin's tumour should be considered. Warthin's tumour presents as a lymphocytic infiltrate and cystic epithelial proliferation. The cysts are lined with a double layer of characteristic eosinophilic epithelial cells (oncocytes) and embedded on a dense lymphoid stroma. Smokers have a high risk of developing Warthin's tumour. On plain CT, Warthin's tumours show hyperdensity and are heterogeneous in nature with high-density haemorrhage and low-density necrosis or cyst. On CT with contrast, Warthin's tumours show high hyperdensity with obvious enhancement. On MRI, Warthin's tumours show iso-low signal on T1-weighted images, but high signal on T2-weighted and gadolinium-enhanced images and are homogeneous in nature. CT is the method of choice for patients with suspected inflammatory disease and for patients contraindicated for MRI, whereas MRI is the method of choice for

patients with palpable masses and strong suspicion that the lesion is a neoplasm. Our extensive routine MRI study requires approximately 15 minutes to obtain all the images and is excellent not only for assessing the extent of a salivary gland tumour and the relationship to the adjacent structures, but also for determining whether the tumour is benign or malignant. MRI gives information on the exact localisation and extent of the lesions and addresses neighbouring structures, hence CT or MRI with a pathology provides accurate diagnosis. Conservative parotidectomy is the most widely accepted surgical treatment for parotid tumour removal.

DECLARATION

No conflicts of interests were declared by authors.

ACKNOWLEDGEMENT

With thanks to the Shanghai 10th People's Hospital of Tongji University, Shanghai, China.

REFERENCES

1. Warthin AS. Papillary cystadenoma lymphomatosum: a rare teratoid of the parotid region. J Cancer Res. 1929;13:116-25.
2. Kim CH. Warthin's tumor of the parotid gland: a case report. J Korean Assoc Oral Maxillofac Surg. 2012;38:366-70. cross ref
3. Djekidel M, Wang P, Piert M, Mukherji SK, Brown RK. Warthin's tumor multimodality imaging. Anatomic and scintigraphy imaging review, including PET-CT and SPECT-CT. OMICS J Radiol. 2013;2:117.
4. De Jager JP, Choy D, Fleming A. Salivary scanning in rheumatoid arthritis with sicca syndrome. Ann Rheum Dis. 1984;43:610-2. cross ref
5. Katz WA, Ehrlich GE, Gupta VP, Shapiro B. Salivary gland dysfunction in systemic lupus erythematous and rheumatoid arthritis. Diagnostic importance. Arch Intern Med. 1980;140:949-51. cross ref
6. Yousem DM, Kraut MA, Chalian AA. Major salivary gland imaging. Radiology. 2000;216:19-29. cross ref
7. Christe A, Waldherr C, Hallett R, Zbaeren P, Thoeny H. MR imaging of parotid tumors: typical lesion characteristics in MR imaging improve discrimination between benign and malignant disease. AJNR Am J Neuroradiol. 2011;32:1202-7. cross ref
8. Wong KT, Ahuja AT, King AD, Yuen EH, Yu SC. Vascular lesions of parotid gland in adult patients: diagnosis with high-resolution ultrasound and MRI. Br J Radiol. 2004;77:600-6. cross ref
9. Eveson JW, Cawson RA. Warthin's tumor (cystadenolymphoma) of salivary glands. A clinicopathologic investigation of 278 cases. Oral Surg Oral Med Oral Pathol. 1986;61:256-62. cross ref
10. Yoo GH, Eisele DW, Askin FB, Driben JS, Johns ME. Warthin's tumor: a 40-year experience at The Johns Hopkins Hospital. Laryngoscope. 1994;104:799-803.
11. Singh AP, Tandon A, Chowdhary A, Mujoo S. Adenolymphoma: A probing entity: Case report and review. J Nat Sci Biol Med. 2013;4:492-6. cross ref
12. Kotwall CA. Smoking as an etiologic factor in the development of Warthin's tumor of the parotid gland. Am J Surg. 1992;164:646-7. cross ref
13. Allegra SR. Warthin's tumor: a hypersensitivity disease? Ultrastructural, light, and immunofluorescent study. Hum Pathol. 1971;2:403-20. cross ref
14. Ungari C, Paparo F, Colangeli W, Iannetti G. Parotid gland tumours: overview of a 10-year experience with 282 patients, focusing on 231 benign epithelial neoplasms. Eur Rev Med Pharmacol Sci. 2008;12:321-5.
15. Thoeny HC. Imaging of salivary gland tumors. Cancer Imaging. 2007;7:52-62. cross ref
16. Kress E, Schulz HG, Neumann T. Diagnosis of diseases of the large salivary glands of the head by ultrasound, sialography and CT-sialography. A comparison of methods [in German]. HNO. 1993;41:345-51.
17. Wittich GR, Scheible WF, Hajek PC. Ultrasonography of the salivary glands. Radiol Clin North Am. 1985;23:29-37.
18. Nguyen BD, Roarke MC. Salivary duct carcinoma with perineural spread to facial canal: F-18 FDG PET/CT detection. Clin Nucl Med. 2008;33:925-8. cross ref
19. Subramaniam RM, Durnick DK, Peller PJ. F-18 FDG PET/CT imaging of submandibular gland oncocytoma. Clin Nucl Med. 2008;33:472-4. cross ref
20. Tan TJ, Tan TY. CT features of parotid gland oncocytomas: a study of 10 cases and literature review. AJNR Am J Neuroradiol. 2010;31:1413-7. cross ref
21. Bryan RN, Miller RH, Ferreyro RI, Sessions RB. Computed tomography of the major salivary glands. AJR Am J Roentgenol. 1982;139:547-54. cross ref
22. Yao HQ, Lin YP. CT and MRI findings of parotid Warthin's tumors. Chinese-German Journal of Clinical Oncology. 2011;10:596-601. cross ref
23. Choi DS, Na DG, Byun HS, Ko YH, Kim CK, Cho JM, et al. Salivary gland tumors: evaluation with two-phase helical CT. Radiology. 2000;214:231-6. cross ref
24. Ikeda M, Motoori K, Hanazawa T, Nagai Y, Yamamoto S, Ueda T, et al. Warthin tumor of the parotid gland: diagnostic value of MR imaging with histopathologic correlation. AJNR Am J Neuroradiol. 2004;25:1256-62.
25. Sakamoto M, Sasano T, Higano S, Takahashi S, Iikubo M, Kakehata S. Usefulness of heavily T(2) weighted magnetic resonance images for the differential diagnosis of parotid tumours. Dentomaxillofac Radiol. 2003;32:295-9. cross ref
26. Joe VQ, Westesson PL. Tumors of the parotid gland: MR imaging characteristics of various histology types. AJR Am J Roentgenol. 1994;163:433-8. cross ref